Effects of Adsorption Site and Surface Stress on Ordered Structures of Oxygen Adsorbed on W(110)

K. E. Johnson,* R. J. Wilson, and S. Chiang
IBM Research Division, Almaden Research Center, 650 Harry Road, San Jose, California 95120-6099
(Received 3 February 1993)

Ordered phases of O on W(110) entail compressive surface stress, the manifestations of which are directly observed for different coverages using scanning tunneling microscopy. Low coverage adsorption results in a gas phase with disordered persistent structures. At higher coverage, ordered phases condense with disordered domains. O adsorption in the two distinct triply coordinated sites of the W(110) unit cell leads to separate domains with the adsorption site exchanged. Annealing relieves compression within high coverage phases by the formation of site-exchange domain superstructures.

PACS numbers: 68.35.Bs, 68.35.Rh, 68.60.Dv, 82.65.My

Atomic scale ordering of adsorbates at surfaces strongly influences heterogeneous chemical reactivity. Models based on measurements using surface diffraction techniques describe well the local periodicity within single domains. But chemisorption and two dimensional (2D) ordering are also strongly influenced by long range periodicity, which accommodates surface misfit, and by short range nonperiodic structures present at domain walls and phase boundaries. An understanding of the structures associated with 2D condensation and coverage dependent phases is crucial to elucidating the fundamental physical origins of adsorbate ordering and phase differentiation. It is precisely such structural details that we have measured for atomic chemisorption on a metal surface in real space using scanning tunneling microscopy (STM).

Oxygen adsorption on tungsten is one of the earliest [1] and most studied model adsorption systems. On the W(110) surface, multiple coverage dependent phases have been successfully identified and characterized by low-energy-electron diffraction (LEED). The three ordered phases, depicted in Fig. 1(a), are (2×1) at coverage $\theta=0.5$ monolayer (ML), (2×2) at $\theta=0.75$ ML, and (1×1) at $\theta=1.0$ ML [2–4]. The phase diagram for this adsorbate system has been carefully studied using LEED spot profile analysis [5], but at intermediate coverages, where phases coexist, the structural details of nucleation and phase boundaries remain equivocal [6]. The growth of the (2×1) phase upon initial oxygen adsorption is an excellent example of condensation from a 2D gas [5] and is a candidate for study of the forces involved in adsorbate ordering. The two higher coverage phases—considered 2D oxides—consist of close-packed O rows along both close-packed substrate directions, and when annealed exhibit additional superstructures in LEED [4]. Although the adsorption site, Fig. 1(b), is known [7], the effect of the site degeneracy on domain formation was not previously understood. Using STM we have directly imaged condensation, phase coexistence, and the atomic structure of single phase domain walls. These results provide new details of adsorbate structure and lead us to conclude that the same forces which establish periodic structures upon initial condensation play an important role in the remarkably regular domain superstructure formed by higher coverage phases.

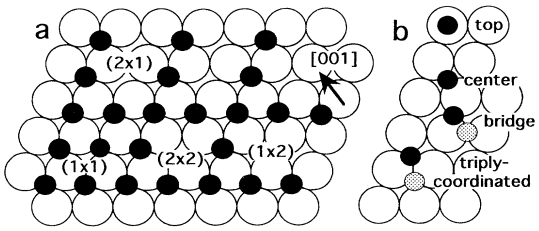

FIG. 1. Model of O adsorbed on W(110). Open circles are the top layer W atoms and filled circles O atoms. (a) Structure of the three ordered phases. (b) Adsorption sites on the W(110) surface; the triply coordinated site is that measured using LEED and confirmed by this study. The two triply coordinated sites will be referred to as right (shaded) and left (solid).

The ultrahigh-vacuum STM system used for these measurements has been described elsewhere [8]. A W(110) thin single crystal was cleaned by repeated cycles of hot oxidation followed by 2200 K flash to remove the oxide. O adsorption for observation by the STM was performed without heating, shortly following the final high temperature flash, but after the sample had cooled to below 700 K. O_2 exposure to between 10^{-7} and 10^{-3} Torr sec generated coverages of 0.1 to 1.0 ML. Changes to the ordered phases after annealing were also investigated. In each case the overlayer structure was confirmed by LEED measurements during or immediately following O_2 exposure or annealing. STM images taken at room temperature (RT) are shown in height keyed gray scale with aspect and skew corrected using the known adsorbate lattice.

The contrast at O adsorption sites can be determined unambiguously using images taken with low coverages, when the (2×1) phase coexists with the 2D gas. From the STM images in Figs. 2(a)-2(c), it is clear that adsorbed oxygen is imaged as a depression. This is predicted by calculation [9] and is similar to observations of O adsorption on other metal surfaces [10,11]. At $\theta\approx 0.1$

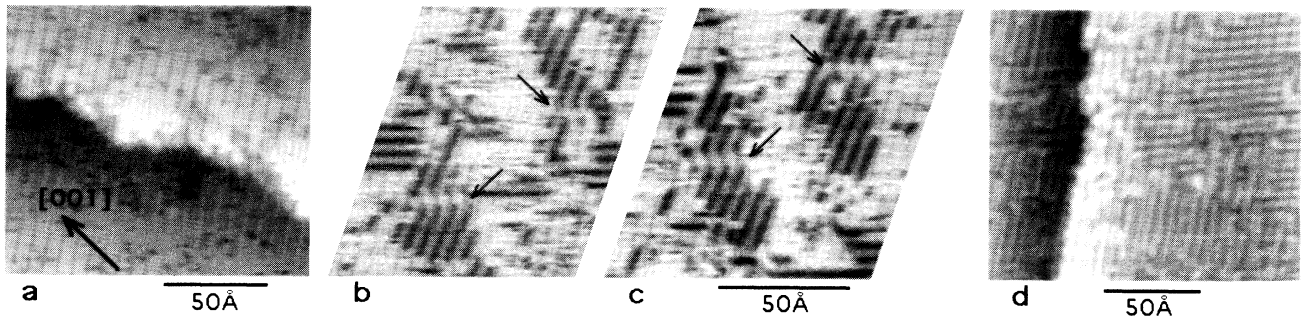

FIG. 2. Low coverage and condensation. Crystallographic orientation is consistent for all images. (a) $\theta \approx 0.1$ ML with adsorption principally as a 2D gas. Nucleation of (2×1) phase at step edges. $i_{\text{tunnel}} = 1$ nA, $V_{\text{sample}} = -0.1$ V. (b) and (c) $\theta \approx 0.2$ ML. Images taken in sequence: Arrows indicate two site-exchange domain walls contained in both images. $i_{\text{tunnel}} = 1$ nA, $V_{\text{sample}} = +0.5$ V. (d) Saturated (2×1) phase at $\theta = 0.5$ ML. $i_{\text{tunnel}} = 1$ nA, $V_{\text{sample}} = +0.1$ V. Measured corrugation of (2×1) rows ≈ 0.4 Å.

ML in Fig. 2(a), stable ordered domains of (2×1) are only observed at step edges. Much of the adsorbate structure on terraces appears oriented not in the close-packed directions of the (2×1) phase but instead in the [001] direction. These short rows of adsorbed O lack long range order. Such structures can persist for hours, but are modified at the ends by evaporating to or condensation from the 2D absorbate gas. Below the coverage that saturates the (2×1) phase, adsorbate features on the terraces change between successive images. At $\theta \approx 0.2$ ML, in Figs. 2(b) and 2(c), (2×1) and (1×2) domains condense on the terraces. These images were taken ≈ 2.5 min apart, during which time existing O islands have grown or dissolved and new islands have nucleated. Again additional single rows of adsorbed O persist in non-close-packed orientations. At RT oxygen atoms adsorbed in the lowest coverage phase are mobile, although we cannot rule out the possible influence of the scanning tip or contamination.

The stable structures indicated in Figs. 2(b) and 2(c) are walls between parallel domains, across which the close-packed rows have shifted 0.25 Å to the right from bottom to top. These walls are 2D partial dislocations, which separate domains where the O adsorption site is exchanged between the triply coordinated site on the left side of the unit cell in the lower domain to the right side in the upper domain. (The evidence by which we confirm the adsorption site is derived from images of all three ordered phases and follows.) We refer hereafter to domains of all phases that are differentiated by the adsorption site in the unit cell as site-exchanged domains. For this phase, the other domain transformations are translation perpendicular to the rows to an antiphase domain and rotation by 109.5° into nonparallel domains, which yield a total of eight possible (2×1) domains.

Figure 2(d) shows the complete (2×1) phase with $\theta = 0.5$ ML. This sample was annealed to 1425 K after adsorption. RT adsorption of $\theta = 0.5$ ML produces initially smaller domains which coarsen upon annealing to this temperature, but the domains do not change further in size or appearance when annealed up to 1750 K. Typical domains are never much larger than 75 Å in any one direction. At RT for all coverages $\theta \geq 0.5$ ML the imaged surface remains unchanged with time.

The progression with increasing coverage to the (2×2) and (1×1) phases is illustrated in Fig. 3. In Fig. 3(a) two nonparallel (2×1) domains are imaged adjacent to a single (2×2) domain. Figure 3(b) is of the nearly complete (2×2) phase; including site exchange, eight possible domains exist for this phase. In Fig. 3(c) the transition to the (1×1) phase is imaged. At both coexistence coverages, adsorbate symmetry lines remain collinear at phase boundaries, indicating no change in adsorption site. The coexistence of (2×1) and (2×2) is characterized by segregated regions of the higher coverage with only a few random sites within the (2×1) containing extra adsorbed O; the (2×2) and (1×1) phases form completely segregated regions. Static and segregated adsorbate phases imply that oxygen is mobile during adsorption. Transport to the phase boundaries may occur either via surface diffusion prior to chemisorption or via displacive motion of regions of higher local density within an existing lower coverage phase.

Figure 3(d) shows the unannealed (1×1) phase with site-exchanged domains. Walls form in the two close-packed directions and the [001] direction. The adsorption site symmetry dictates that domain walls alternate between heavy and light; examples of atomic structure at both types of domain walls are shown in Fig. 4. We infer the following rules for site filling at domain walls; One W atom may have up to four adjacent O atoms, but only a single O atom may occupy the long hollow of one unit cell. Prior to annealing, the domain boundaries are disordered and therefore give rise to no additional diffraction features in LEED.

Annealing the (1×1) phase causes a remarkable ordering of the site-exchanged domains into the superstructure shown in Fig. 5. The ≈ 20 Å wide corrugated stripes are single domains. The regularly spaced parallel domain walls are aligned in the $[1\bar{1}3]$ direction; other regions on

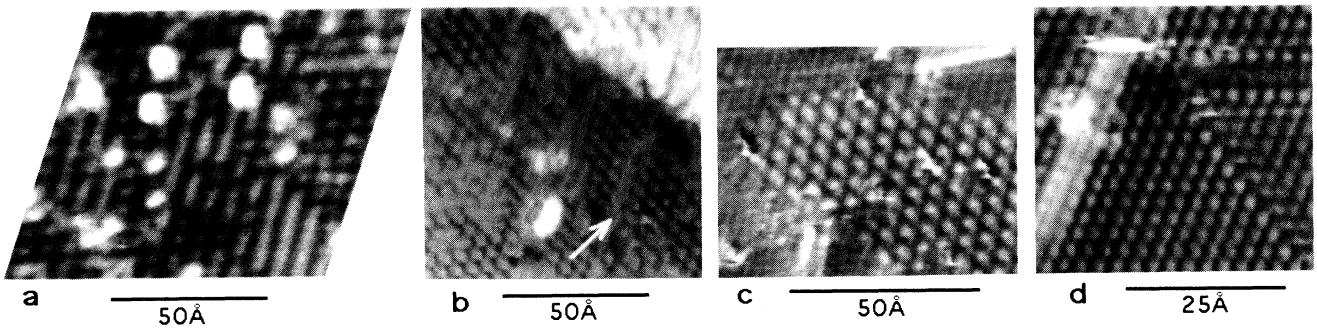

FIG. 3. Growth of 2D oxide phases. (a) Coexistence of (2×1) with (2×2). (2×1) in lower right and (1×2) in upper right with intervening (2×2) domain all have same adsorption site. $i_{\text{tunnel}}=1$ nA, $V_{\text{sample}}=+0.2$ V. (b) Nearly complete (2×2) at $\theta\approx 0.75$ ML. Arrow indicates a site-exchange domain wall. $i_{\text{tunnel}}=2$ nA, $V_{\text{sample}}=-0.3$ V. (c) Coexistence of (2×2) in center with surrounding (1×1). $i_{\text{tunnel}}=2$ nA, $V_{\text{sample}}=-45$ mV. (d) Saturated $\theta=1$ ML (1×1). $i_{\text{tunnel}}=1$ nA, $V_{\text{sample}}=-10$ mV. Measured corrugations are ≈ 1.4 Å for (2×2) and ≈ 0.7 Å for (1×1).

the sample show alignment in the [$\bar{1}$13] direction. The width of the walls alternates, a consequence of the site-exchange domains. The regular periodicity and orientation of the walls give rise to the extra superstructure diffraction features, which had been previously interpreted as arising from a compressed misfit overlayer [4,12]. Prior to acquiring the image shown here with apparently tall domain walls 1–3 atomic spacings wide, the sample was annealed to 1250 K. We expect that this annealing temperature has desorbed some of the oxygen [4], preferentially uncovering W at the domain walls and giving rise to the width and apparent height of the walls. If instead the RT (1×1) phase is annealed to a lower temperature, 1050 K, narrower abrupt walls form. Annealing a sample with $\theta=0.75$ ML forms a similar superstructure of (2×2) site-exchanged domains, which include the additional four translational domains possible for this phase.

STM can confirm the O adsorption site [7] without directly imaging the substrate metal corrugation by examining domain structures and eliminating likely adsorption sites, shown in Fig. 1(b). The presence of two (1×1) domains in Fig. 3(d) implies an adsorption site with symmetry different than the substrate; this trivially eliminates the top and center sites. Concrete evidence distinguishing the bridge and triply coordinated adsorption sites is found when considering the symmetry restrictions of the (2×1) phase. The bridge site lies above the W close-packed rows, and therefore the two close-packed directions are not degenerate. Adsorption into the bridge site would require that parallel (2×1) domains always occupy the same site in the unit cell, and nonparallel domains would then constitute site exchange. These restrictions contradict the site-exchange domain walls observed for the (2×1) phase in Figs. 2(b) and 2(c), as well as the existence of a single (2×2) domain aligned with two non-

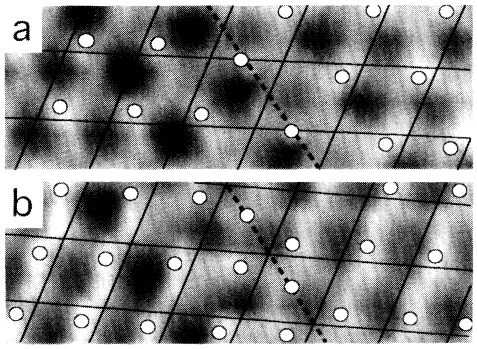

FIG. 4. Site-exchange (1×1) domain walls in [001] direction. Images are inverted. Solid lines indicate substrate lattice, broken line the domain wall, and open circles the O adsorption site. (a) Light wall with local site density less than in domain, and (b) heavy wall with greater density. At both types of walls an additional row of O adsorbs between domains in an intermediate site.

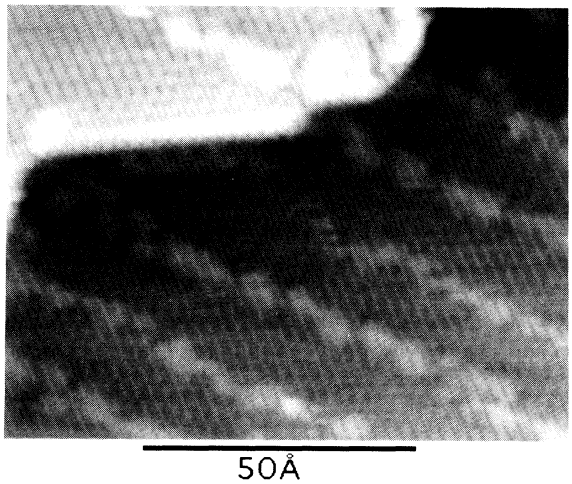

FIG. 5. Superstructure of site-exchanged (1×1) domains. STM image after anneal to 1250 K. $i_{\text{tunnel}}=1$ nA, $V_{\text{sample}}=+1$ V. Domain corrugation ≈ 0.3 Å with walls ≈ 0.6 Å tall.

parallel (2×1) domains—Fig. 3(a) with schematic in Fig. 1(a). From this evidence we conclude that all domains which are not related by simple lattice translation are from site exchange between the two triply coordinated sites, with partial dislocations of the overlayer atomic lattice at the domain walls. The 2D space group for the adsorbate-substrate unit cell is $c1m1$.

Collectively these data provide insight into the condensation and ordering of adsorbates. The (2×1) phase does not spontaneously condense at the lowest O coverages except at step edges. When the 2D gas pressure is increased by higher coverage, an equilibrium is established and the (2×1) phase condenses on terraces; Figs. 2(b) and 2(c). The low density structures aligned in the [001] direction are stable only in the 2D gas at $\theta < 0.5$, but may serve as nucleation sites for (2×1) islands. In the condensed (2×1) phase, the density of O atoms along the close-packed direction generates compressive stress, but ordering between rows is driven by a longer range attractive force. This also explains the formation of the (2×2) phase; the addition of O atoms between rows increases the close-packed compressive stress, but also adds an attractive interaction. The (1×1) phase, with the highest degree of compressive stress, forms last.

The altered domain structure observed after annealing all ordered phases accommodates the compressive surface stress. The saturated (2×1) phase generates walls between nonparallel, antiphase, and site-exchanged domains. At each type of domain wall, the close-packed adsorbate rows terminate relieving the stress. During coarsening for this phase, the free energy gained by reducing the boundary length on individual domains is offset by the cost that results from compressive stress associated with increasing domain area; this limits the ultimate domain size for this phase.

Stress in the (2×1) phase is unidirectional, unlike the higher coverage 2D oxides. For these denser phases, stress cannot be relieved by translation or directional domains. The RT (2×2) and (1×1) adsorbate phases with random domain walls are kinetically metastable. Stress is accommodated upon annealing by formation of regularly spaced site-exchanged domains. The direction and spacing of the superstructure domain walls limit the length of close-packed rows in both directions to ≈ 10 atoms. The direction and size of the superstructure domains remain constant for (1×1) and (2×2) 2D oxides, and the unsaturated domain walls in the annealed $\theta = 1$ superstructure in Fig. 5 appear devoid of oxygen. That the superstructure periodicity is independent of local and average coverage implies that stress relaxation is mediated through the substrate. This type of surface relaxation is similar to that observed in the clean surface herringbone reconstruction on Au(111) [13], and explained by calculation of stress domains [14].

Ordered adsorption of O on W(110) generates compressive surface stress. At the lowest coverages, adsorbate ordering requires a 2D condensation pressure from the 2D gas phase. At higher coverages, adsorbate superstructures are simply site-exchanged domains with long range order. Three principal causes can be cited for the formation of long range ordering of domains: internal compressive stress in the close-packed direction, the degenerate adsorption site, and substrate mediated long range interactions. In light of these results, models explaining structural accommodation of surface stress for any adsorbate—including epitaxial metal—must be reexamined based on a model of regularly shifted domain formation. Neither diffraction, with inherent limitations of spatial averaging and model dependent interpretation of local atomic structure, nor local structural probes (e.g., photoelectron diffraction or surface extended x-ray absorption fine structure), which cannot link local structure to long range ordering, are capable of measuring the details of 2D ordering and atomic motion we present herein. Concurrent measurement of local nonperiodic atomic structure with longer range phase and domain ordering requires an atomic scale scanning probe technique and can elucidate the origins of the structure and ordering for adsorbates on surfaces.

This work was supported in part by the Office of Naval Research (N00013-89-C-0099).

*Present address: Department of Chemistry, Goucher College, Baltimore, MD 21204.

[1] I. Langmuir, J. Am. Chem. Soc. **35**, 105 (1913).
[2] L. H. Germer and J. W. May, Surf. Sci. **4**, 452 (1966).
[3] T. Engel, H. Niehus, and E. Bauer, Surf. Sci. **52**, 237 (1975).
[4] E. Bauer and T. Engel, Surf. Sci. **71**, 695 (1978).
[5] P. K. Wu, M. C. Tringides, and M. G. Lagally, Phys. Rev. B **39**, 7595 (1989).
[6] M. C. Tringides, Phys. Rev. Lett. **65**, 1372 (1990).
[7] M. A. Van Hove and S. Y. Tong, Phys. Rev. Lett. **35**, 1092 (1975).
[8] S. Chiang, R. J. Wilson, Ch. Gerber, and V. M. Hallmark, J. Vac. Sci. Technol. A **6**, 386 (1988).
[9] N. D. Lang, Comments Condens. Matter Phys. **14**, 253 (1989).
[10] J. A. Meyer, Y. Kuk, P. J. Estrup, and P. J. Silverman, Phys. Rev. B **44**, 9104 (1991).
[11] R. J. Behm, in *Scanning Tunneling Microscopy and Related Methods*, edited by R. J. Behm, N. Garcia, and H. Rohrer (Kluwer Academic, The Netherlands, 1990), p. 173.
[12] E. Bauer, Surf. Sci. **7**, 351 (1967).
[13] Ch. Wöll, S. Chiang, R. J. Wilson, and P. H. Lippel, Phys. Rev. B **39**, 7988 (1989).
[14] S. Narasimhan and D. Vanderbilt, Phys. Rev. Lett. **69**, 1564 (1992).

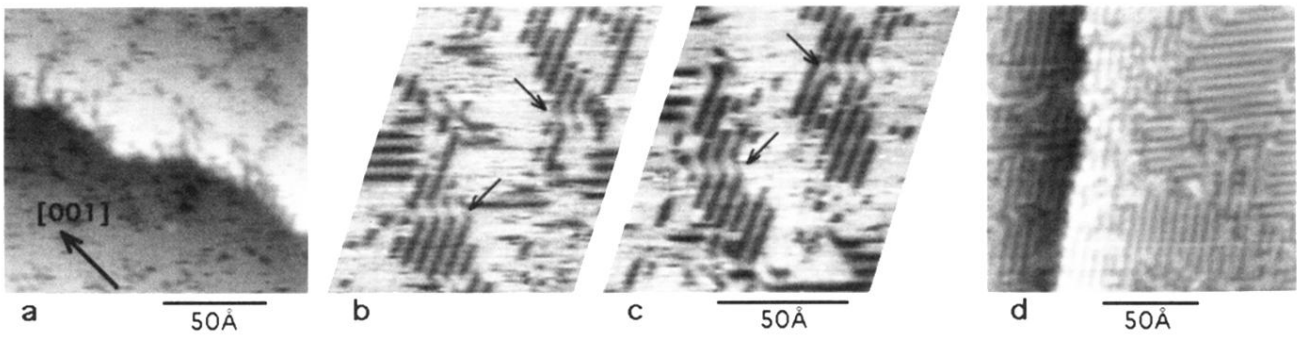

FIG. 2. Low coverage and condensation. Crystallographic orientation is consistent for all images. (a) $\theta \approx 0.1$ ML with adsorption principally as a 2D gas. Nucleation of (2×1) phase at step edges. $i_{\text{tunnel}} = 1$ nA, $V_{\text{sample}} = -0.1$ V. (b) and (c) $\theta \approx 0.2$ ML. Images taken in sequence: Arrows indicate two site-exchange domain walls contained in both images. $i_{\text{tunnel}} = 1$ nA, $V_{\text{sample}} = +0.5$ V. (d) Saturated (2×1) phase at $\theta = 0.5$ ML. $i_{\text{tunnel}} = 1$ nA, $V_{\text{sample}} = +0.1$ V. Measured corrugation of (2×1) rows ≈ 0.4 Å.

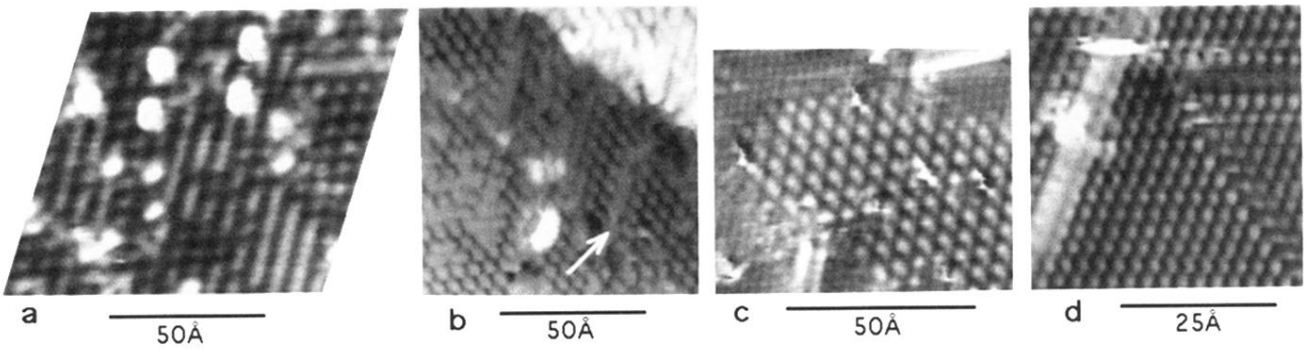

FIG. 3. Growth of 2D oxide phases. (a) Coexistence of (2×1) with (2×2). (2×1) in lower right and (1×2) in upper right with intervening (2×2) domain all have same adsorption site. $i_{\text{tunnel}}=1$ nA, $V_{\text{sample}}=+0.2$ V. (b) Nearly complete (2×2) at $\theta\approx 0.75$ ML. Arrow indicates a site-exchange domain wall. $i_{\text{tunnel}}=2$ nA, $V_{\text{sample}}=-0.3$ V. (c) Coexistence of (2×2) in center with surrounding (1×1). $i_{\text{tunnel}}=2$ nA, $V_{\text{sample}}=-45$ mV. (d) Saturated $\theta=1$ ML (1×1). $i_{\text{tunnel}}=1$ nA, $V_{\text{sample}}=-10$ mV. Measured corrugations are ≈ 1.4 Å for (2×2) and ≈ 0.7 Å for (1×1).

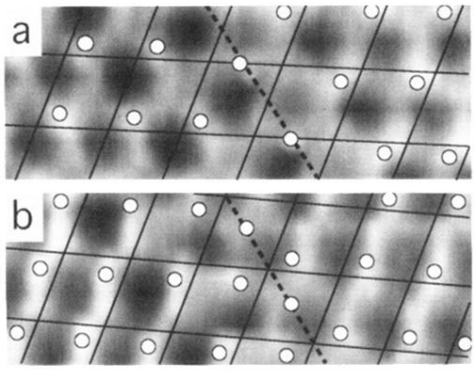

FIG. 4. Site-exchange (1×1) domain walls in [001] direction. Images are inverted. Solid lines indicate substrate lattice, broken line the domain wall, and open circles the O adsorption site. (a) Light wall with local site density less than in domain, and (b) heavy wall with greater density. At both types of walls an additional row of O adsorbs between domains in an intermediate site.

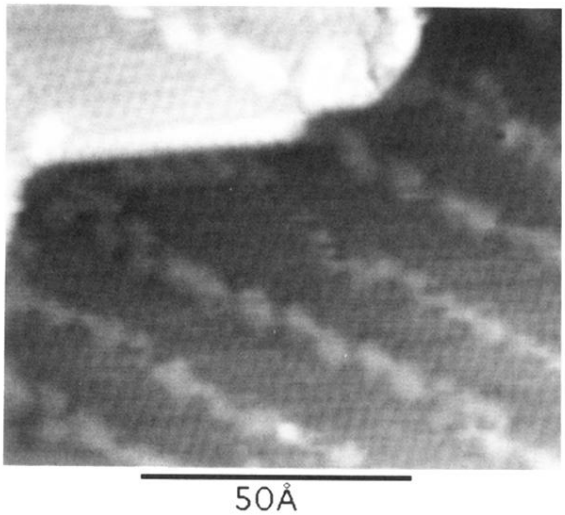

FIG. 5. Superstructure of site-exchanged (1×1) domains. STM image after anneal to 1250 K. $i_{\text{tunnel}}=1$ nA, $V_{\text{sample}}=+1$ V. Domain corrugation ≈ 0.3 Å with walls ≈ 0.6 Å tall.